Active Nematics with Integer Defects in Active Colloids of Ellipsoidal Rollers

Bao Ying Fan(樊宝营),[1] Lin Liu(刘霖),[1] Jie Wu(邬杰),[1] Chen Song(宋辰),[1] Wen-de Tian(田文得),[1]Kang Chen(陈康),[1]
Tian Hui Zhang(张天辉)[1]*

1.Center for Soft Condensed Matter Physics and Interdisciplinary Research & School of Physical Science and Technology, Soochow University, Suzhou, 215006, China

Corresponding authors: Tian Hui Zhang: zhangtianhui@suda.edu.cn ,
Wen-De Tian: tianwende@suda.edu.cn,
Kang Chen: kangchen@suda.edu.cn

Abstract

How propulsion direction relative to particle shape controls topological ordering remains unclear. Here, we study dense ellipsoidal Quincke rollers driven perpendicular to their long axes. It is found that under a high-frequency alternating current (AC) electric field, large-scale polar order emerges through the merging of local nematic domains. Unlike conventional active nematics dominated by half-integer defects, the transversely driven prefers integer defects: $+1$ vortices with radially aligned particle axes and -1 saddle defects with fourfold symmetry. These defects are confined in domain walls, along which oppositely charged pairs approach and annihilate. These results demonstrate that a polar velocity field can coexist with a perpendicular nematic body axis. This coupling produces unconventional defect textures and a distinct route to global ordering. Our findings offer a robust protocol that the angle between propulsion and polar axis as a practical parameter for controlling topological properties of active nematics.

Keywords: active nematics, ellipsoidal Quincke roller, topological defect

PACS: 64.60.-i, 05.65.+b, 87.18.Gh, 82.70.Dd

Introduction

Collective motion [1–4] is one of the most prominent manifestations of active matter emerging in systems such as cytoskeletal assemblies,[5] bacterial suspensions, [6–8]animal groups [9–11] and synthetic microswimmers. [12] A central theme in active-matter physics is to understand how microscopic propulsion and the interactions between active units determine macroscopic behaviors. To explore the general principles underlying various collective motions, observations have been conducted in various model systems. Among these systems, elongated bacteria and actin filaments, [13] which are modeled as a collection of rod-like active particles, [14] have been widely studied both theoretically and experimentally as models of active nematics with long-range orientational order. [14]Active nematics represent a class of nonequilibrium materials which have no equilibrium counterpart. More importantly, active nematics offer a robust model in understanding collective cell migration, [15] intracellular organization and biological pattern formation. [16] The role of topological defects in active nematics is also of fundamental importance in controlling morphogenesis and extrusion events. [17,18]

In two-dimensional nematic phases, [14,19,20] the head-tail symmetry of the director field makes directions $\mathbf{n}$ and $-\mathbf{n}$ equivalent, and the lowest-energy topological defects are half-integer: comet-like +1/2 defects and trefoil-like -1/2 defects. Around the +1/2 defects, the asymmetric distortion of the nematic field creates unbalanced active stresses which propel them to move as self-propelled particles. The three-fold symmetry of the nematic field around the -1/2, the active stresses are balanced at their core, leading to zero net self-propulsion. [20–22] They typically move with surrounding flows. Defects with opposite-charge annihilate or are created in pair. The continuous creation, motion, and annihilation of defects leads to a chaotic, turbulent-like state even at low

Reynolds numbers. The motion of +1/2 defects is a primary driver of the flow field, acting as local force dipoles that stir the fluid. [20]

So far, the popular understanding of topological defects and active nematic is based on the model that the active rod-like units are propelled along the long axis such that the polar orientation of active rods and the directions of propulsion or velocity are intrinsically coupled. [14,15,23] In this case, active stress produces an active force which propels the $+1/2$ defect along the polar axis. Despite of its fundamental importance, the question that if active rods are propelled perpendicular to their long axes, what kind of topological defects will form and how they will move in active nematics? Here, in this study, ellipsoidal Quincke rollers are employed as a model system, where active ellipsoids are driven transversely along their short axes. [24] Distinct from previous studies of active ellipsoidal Quincke rollers, [24–26] dense suspensions of ellipsoidal Quincke rollers in this study develop large-scale polar order with integer topological defects rather than half-integer defects. These defect structures differ from those in the conventional polar phase, where +1 defects feature particles aligning tangentially. Instead, +1 defects in our system possess a radial vortex configuration, with particle long axes strictly pointing radially toward or away from the defect core, while −1 defects exhibit saddle-point structures with fourfold symmetry. Furthermore, domain walls provide pathways for topological defect motion. Driven by elastic attractive interactions between oppositely charged defects, +1 and −1 defects migrate along these domain walls toward each other and annihilate, substantially enhancing the efficiency of system ordering.

Results

Ellipsoidal Quincke rollers driven by a direct current (DC) electric field exhibit two different states: Near the critical field, the rollers exhibit a strong chirality due to the tilted spinning axis and

the resulted processing.[24] Increasing the spinning angular speed can suppress the processing. Distinct from rod-like particles propelled along the long axes, ellipsoidal Quincke rollers are propelled along the short axes such that two rollers moving with opposite velocities block each other although their long axes are parallel, giving rise to clustering rather than aligning in collision.[24] Near the critical field, ellipsoidal Quincke rollers can align their velocities by flipping[25] to form small-scale polar fluid with nematic order. However, the flocking near the critical field is not stable because of the strong chirality of ellipsoidal Quincke rollers. Recently, however, we found that a high-frequency alternating current (AC) electric field can effectively suppress the chirality and facilitate the formation of large-scale polar fluid.[26]

Figure 1 exhibits a typical emergence of large-scale polar fluid of ellipsoidal Quincke rollers (Figs.1(a)-1(c)). To quantify the polar order, the local polar order parameter $\boldsymbol{P}$ is calculated with the velocities of individual rollers (see Methods). It shows that the initial polar order emerges locally as small-scale polar domains (Fig. 1(d)). The polar domains grow by aligning surrounding rollers (Fig.1(e)). A globally ordered polar phase is achieved by the merging of polar domains (Fig. 1f). In the growth and merging of polar domains, flipping-mediated alignment of ellipsoidal rollers[26] plays a key role. Accompanying the formation of polar domains, ellipsoidal rollers are aligned along the long axis simultaneously. In this case, the nematic orientation (Fig.1(c)) is perpendicular to the orientation of polar order (Fig.1(f)).

At the boundaries between polar domains, the mismatch of polar orientations results in the distortion of polar field and therefore the formation of topological defects. To quantify spatial distortions of the polar field, the local strain magnitude $|\nabla \boldsymbol{P}|$ is defined and calculated with the velocities of individual rollers (see Methods). Ellipsoidal rollers in different domains are

characterized by different directions of velocities as well as nematic orientations. Therefore, $\boldsymbol{P}$ experiences an abrupt change in the velocity direction across the boundaries between different domains, thereby producing extremely high polar gradient values $|\nabla \boldsymbol{P}|$. As a result, the gradient field $|\nabla \boldsymbol{P}|$ offers a measurement of the magnitude of local distortion of polar field. [27] The maximal points in the polar gradient field locate the positions of topological defects. In the colored field of $|\nabla \boldsymbol{P}|$, the centers of topological defects can be clearly identified at the domain walls. At the early state as the number of defects is large, the interconnected domain walls form a network in the system (Fig.2(a)). Accompanying the growth of the scale of polar order, the number of defects decreases due to annihilation and the network breaks up into segments (Figs.2(b) and 2(c)). Two types of topological defects, rotational vortex-like (Fig. 2(d)) and diagonal saddle-like (Fig. 2(e)), are identified. In the vortex-like defects, the orientation of velocity or long axis of rollers changes 2π (Fig. 2(d)) after a full circle rotation while in the saddle-like defects, it changes -2π (Fig. 2(e)). These two types of defects correspond to $+1$ and -1 defects. In a $+1$ defect, the velocity field forms a vortex while the long axes align radially. This structure contrasts sharply with the azimuthal alignment typically observed in cell systems. [28] The -1 defect exhibits a saddle-like flow structure with fourfold symmetry.

In the development of globally ordered phase, the total defect number decreases monotonically (Fig. 3(a)) while the global polar order parameter increases (Fig. 3(b)). The synchronous decrease in the number of $+1$ and -1 defects indicates that defect reduction is not a random process, but rather a process of pairwise annihilation. Figure 4 shows that the motion of ± 1 defects is confined to domain walls. The network of domain walls therefore restricts defect motion from two-dimensional planes to one-dimensional lines. Guided motion substantially enhances the efficiency of oppositely

charged defects meeting and annihilating. In active bacteria and cells, the +1/2 defect is propelled by the unbalanced stress [29] while the $-1/2$ defect can only move due to the interaction between defects. In our study, both the $+1$ defects and -1 defects have a symmetry structure, and the surrounding stresses are balanced. Therefore, they are not propelled and can only move by interactions. In the absence of propulsion, the motion of defects is confined within the domain walls. Defects as singularities of the order parameter field imply local orientational distortion, producing significant strain gradients and accumulating elastic energy in the system. [19] The system always tends to minimize the total elastic energy to reach a more stable state. When a pair of topologically opposite defects (± 1) coexist, their respective strain fields can partially cancel in space. By approaching each other, this pair of defects can significantly reduce the degree of elastic deformation in the entire system, thereby lowering the total free energy, giving rise to an attraction between $+1$ defects and -1 defects. Driven by attractive interaction, $+1$ defects and -1 defects tend to meet and annihilate, giving rise to larger polar domains (Fig.4).

The above results show that the direction of propulsion relative to the particle's asymmetry shape is also a key control parameter for topological ordering in active nematics. Although the ellipsoidal rollers possess a nematic body axis, they propel perpendicular to this axis and form a polar velocity field. The system therefore combines transverse nematic alignment with polar motion, and its ordering dynamics is governed by integer $+1$ and -1 defects. This behavior differs from conventional active nematics, where propulsion and particle orientation are usually coupled and the dominant defects have charges $+1/2$ and $-1/2$. [14,29] The polar $+1/2$ defect self-propels through asymmetric active stresses, promoting persistent defect creation, annihilation, and active turbulence. The $+1$ and -1 defects are not propelled due to the balanced stress, and their motion is confined

along domain walls, where oppositely charged defects approach by attraction and annihilate.

The wall-guided annihilation resembles the topology-driven ordering reported for spherical Quincke rollers.[27] However, spherical rollers have no independent body axis. In our ellipsoidal system, the velocity and particle orientation remain perpendicular: a $+1$ velocity vortex is accompanied by radial alignment of the particle long axes, while the -1 defect exhibits a fourfold saddle texture. This microscopic structure is unique to transverse propulsion and cannot occur in isotropic roller flocks. Integer defects have also been studied in cell monolayers[28,30] and bacterial suspensions[31] where they are commonly stabilized by confinement or patterned substrates and may split into half-integer defects. In contrast, the defects observed here arise spontaneously in the bulk, migrate along evolving domain walls, and disappear through pair annihilation.

Conclusion

In summary, we have shown that dense ellipsoidal Quincke rollers driven perpendicular to their long axes develop large-scale polar order through defect-mediated coarsening. The polar velocity field coexists with a perpendicular nematic particle orientation and supports integer $+1$ vortex and -1 saddle defects. The $+1$ defects exhibit a distinctive structure in which the velocity circulates around the core while the particle long axes align radially. During ordering, oppositely charged defects migrate along domain walls and annihilate, weakening the walls and merging neighboring polar domains. The simultaneous decrease in defect number and increase in polar order directly link defect removal to global ordering. These results show that defect topology is determined not only by particle shape, but also by the direction of propulsion relative to that shape. This provides a concrete design principle for anisotropic active colloids: changing the propulsion geometry can select defect structures and alter the pathway and rate of collective ordering.

Materials and Methods

Preparation of ellipsoidal particles. The preparation of the ellipsoidal Quincke roller system follows the protocol established by Bricard et al. [32] Polystyrene spheres (Thermo Scientific G1000) with a radius of R = 10.1 μm are stretched into ellipsoidal particles according to the methods reported by Keville [33] and Ho [34]. Despite variations in aspect ratio, all ellipsoidal particles retain an identical volume.

Experimental Setup. Ellipsoidal Quincke particles with an aspect ratio of k≈1.65 are uniformly dispersed in a 0.12 mol/L sodium bis (2-ethylhexyl) sulfosuccinate (AOT)/hexadecane solution and subsequently injected into a sealed cell assembled by two parallel indium tin oxide (ITO) conductive glass plates. The effective thickness of this cell is 110 ± 10μm. An external electric field perpendicular to the electrode surface is applied.

Polar Order Parameter.

$$\boldsymbol{P} = \frac{1}{N}\left|\sum_{i=1}^{N}\frac{\overrightarrow{v_i}}{|\overrightarrow{v_i}|}\right|$$

The local polar order parameter is defined for individual particles. It is calculated with the directions of velocities of all concerned particles. The summation is over one particle and all its neighbor particles identified by Voronoi diagram.

Local strain magnitude.

$$|\nabla \boldsymbol{P}| = \sqrt{(\frac{\partial p_x}{\partial x})^2 + (\frac{\partial p_x}{\partial y})^2}$$

References

[1] Shelke Y, S A N, and Vutukuri H R 2026 *Science* **392** 202

[2] Sariyar Y, Akduman A U, Negro G, and Carenza L N 2026 *Nat. Commun.* **17** 3289

[3] Zheng Z, Jiang C, Chen Y, Baggioli M, and Zhang J 2026 *Proc. Natl. Acad. Sci. U.S.A.* **123** e2510873123

[4] Gompper G et al. 2025 *J. Phys.: Condens. Matter* **37** 143501

[5] Das M, Schmidt C F, and Murrell M 2020 *Soft Matter* **16** 7185

[6] Turiv T et al. 2020 *Nat. Phys.* **16** 481

[7] Wu J et al. 2025 *Nat. Commun.* **16** 10605

[8] Be'er A and Ariel G 2019 *Mov. Ecol.* **7** 9

[9] Katz Y, Tunstrøm K, Ioannou C C, Huepe C, and Couzin I D 2011 *Proc. Natl. Acad. Sci. U.S.A.* **108** 18720

[10] Ballerini M et al. 2008 *Proc. Natl. Acad. Sci. U.S.A.* **105** 1232

[11] Cavagna A, Cimarelli A, Giardina I, Parisi G, Santagati R, Stefanini F, and Viale M 2010 *Proc. Natl. Acad. Sci. U.S.A.* **107** 11865

[12] Deseigne J, Dauchot O, and Chatè H 2010 *Phys. Rev. Lett.* **105** 098001

[13] Huber L, Suzuki R, Krüger T, Frey E, and Bausch A R 2018 *Science* **361** 255

[14] Doostmohammadi A, Ignés-Mullol J, Yeomans J M, and Sagués F 2018 *Nat. Commun.* **9** 3246

[15] Doostmohammadi A and Ladoux B 2022 *Trends Cell Biol.* **32** 140

[16] Maroudas-Sacks Y, Garion L, Shani-Zerbib L, Livshits A, Braun E, and Keren K 2021 *Nat. Phys.* **17** 251

[17] Brézin L, Risler T, and Joanny J-F 2022 *Eur. Phys. J. E* **45** 30

[18] Zhao Z, Li H, Yao Y, Zhao Y, Serra F, Kawaguchi K, Zhang H, and Sano M 2025 *Nat. Commun.* **16** 2452

[19] Frank F C 1958 *Discuss. Faraday Soc.* **25** 19

[20] Giomi L, Bowick M J, Ma X, and Marchetti M C 2013 *Phys. Rev. Lett.* **110** 228101

[21] DeCamp S J, Redner G S, Baskaran A, Hagan M F, and Dogic Z 2015 *Nature Mater.* **14** 1110

[22] Genkin M M, Sokolov A, Lavrentovich O D, and Aranson I S 2017 *Phys. Rev. X* **7** 011029

[23] Dunkel J, Heidenreich S, Drescher K, Wensink H H, Bär M, and Goldstein R E 2013 *Phys. Rev. Lett.* **110** 228102

[24] Chen Y, Wang L, and Zhang T H 2023 *Soft Matter* **19** 512

[25] He K X, Ni Q Y, Zhou X Y, Tian W D, Chen K, and Zhang T H 2025 *Chinese Phys. B* **34** 076401

[26] Liu L, Wu J, Song C, Chen K, Tian W-D, and Zhang T H 2026 *Acta Phys. Sin.* **75**

[27] Chardac A, Hoffmann L A, Poupart Y, Giomi L, and Bartolo D 2021 *Phys. Rev. X* **11** 031069

[28] Endresen K D, Kim M, Pittman M, Chen Y, and Serra F 2021 *Soft Matter* **17** 5878

[29] Giomi L, Bowick M J, Mishra P, Sknepnek R, and Marchetti M C 2014 *Phil. Trans. R. Soc. A* **372** 20130365

[30] Blanch-Mercader C, Guillamat P, Roux A, and Kruse K 2021 *Phys. Rev. E* **103** 012405

[31] Peng C, Turiv T, Guo Y, Wei Q-H, and Lavrentovich O D 2016 *Science* **354** 882

[32] Bricard A, Caussin J B, Desreumaux N, Dauchot O, and Bartolo D 2013 *Nature* **503** 95

[33] Keville K M, Franses E I, and Caruthers J M 1991 *J. Colloid Interface Sci.* **144** 103

[34] Ho C C, Keller A, Odell J A, and Ottewill R H 1993 *Colloid Polym. Sci.* **271** 469

Competing interests:
All other authors declare that they have no competing interests.

Data availability:
The data supporting this article have been included as part of the Supplementary Information.

Acknowledgments

K.C., W.T. and T.H.Z. acknowledge financial support of the National Natural Science Foundation of China (Grant 12574230 to T.H.Z.; Grants 21774091and 22673081 to K.C.; Grants 21674078 to W.T.).

Author contributions:
T.H.Z., K.C. and W.T. designed the experiment. B. Y. F, L. L, C.S and J. W performed the research and contributed equally. K.C., W.T. and T.H.Z. analyzed the data and wrote the paper.

Figures

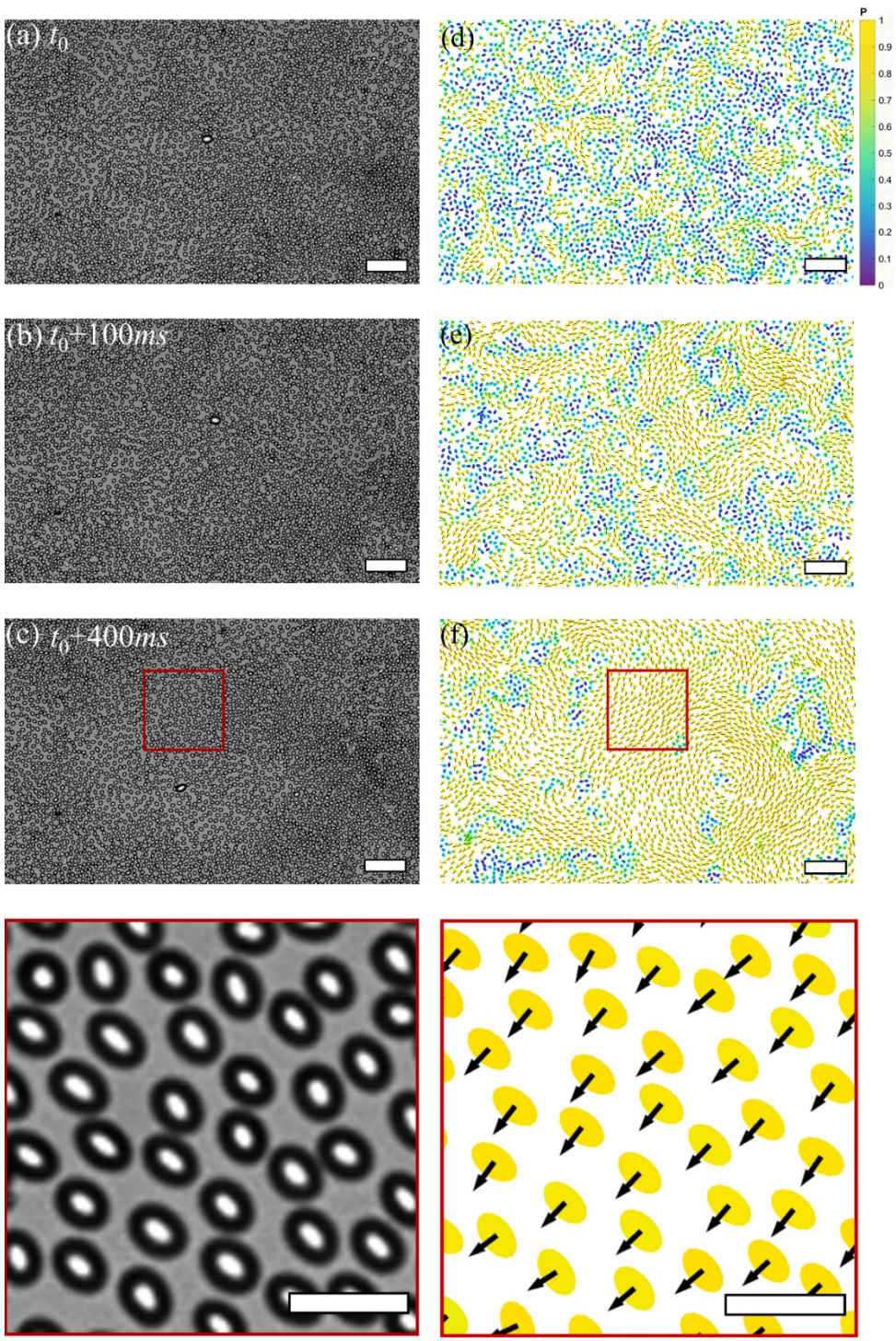


Fig.1 The evolution process from a disordered state to a large-scale coherent state under an AC electric field. The field parameters were set as a peak electric field $E_p/E_c = 2.3$, ground electric field $E_g = 0$, and frequency $f = 130Hz$, where E_c is the critical electric field. (a-c) Snapshots of Ellipsoidal rollers. (d-f)

Evolution of the polar order parameter $\boldsymbol{P}$ corresponds to (a-c). The scatter colors represent the local polarization order parameter $\boldsymbol{P}$ with the color gradient from blue to yellow indicating the increase of local alignment degree from 0 (random) to 1 (highly aligned), and the black arrows denote the velocity directions of the particles. The scale bars in (a–f) are 100 μm. The scale bars in the insets of (c) and (f) are 20 μm.

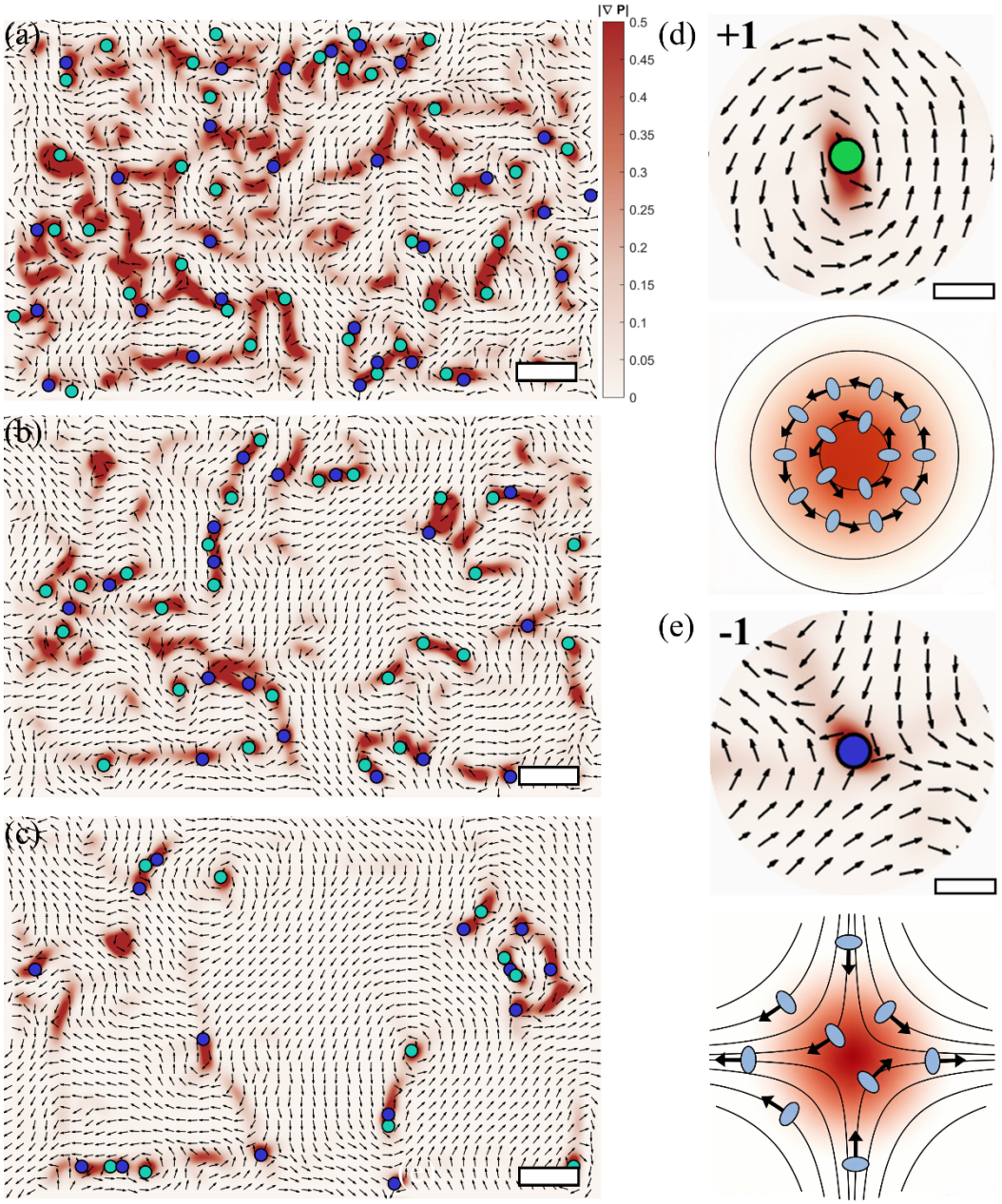


Fig.2 Evolution of the local strain magnitude$|\nabla \boldsymbol{P}|$. (a-c) Time evolution of polarization strain field$|\nabla \boldsymbol{P}|$. The brick-red regions indicate the maxima of the magnitude of the strain field$|\nabla \boldsymbol{P}|$, corresponding to domain walls between differently oriented domains. The black arrows denote the local velocity vector directions. (d) +1 Defect. The core of the green singular point exhibits a characteristic vortex-like structure, with the velocity vector rotating continuously by 2π around the center. (e) -1 Defect. The core of the blue singular point exhibits a characteristic saddle-point-like structure, with the velocity vector displaying a hyperbolic flow manifold. The scale bars in (a–c) are100 μm. The scale bars in (d-e) are 50 μm.

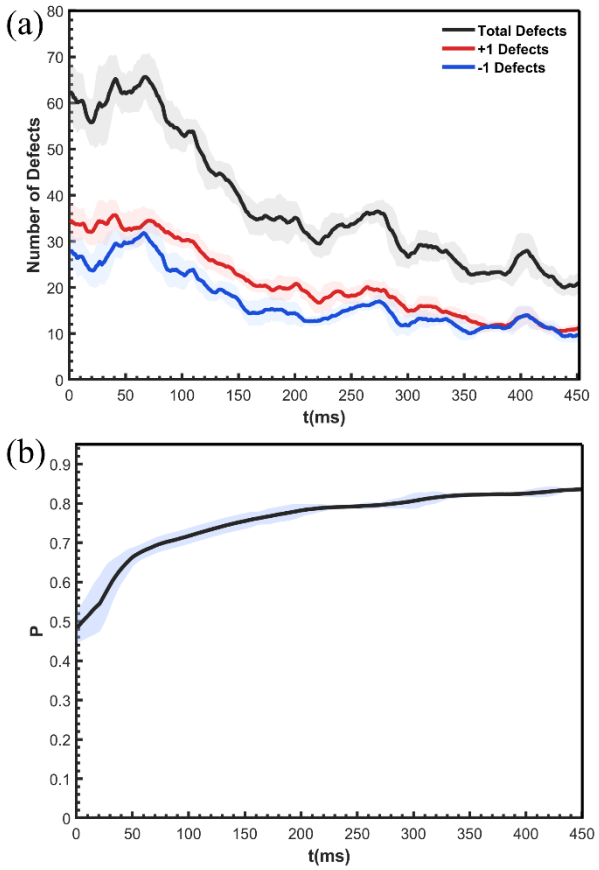


Fig.3 Evolution curves of topological defect number and polarization order parameter over time. (a) Temporal evolution of the total number of topological defects (black), along with the numbers of +1 charged (red) and −1 charged (blue) defects. The shaded regions of the curves represent error bands. The numbers of +1 and −1 defects remain closely consistent throughout the evolution, indicating that oppositely charged defects annihilate in pairs. (b) The polarization order parameter increases over time. The shaded region of the curve represents the error band. Shaded regions are calculated from 100 samples.

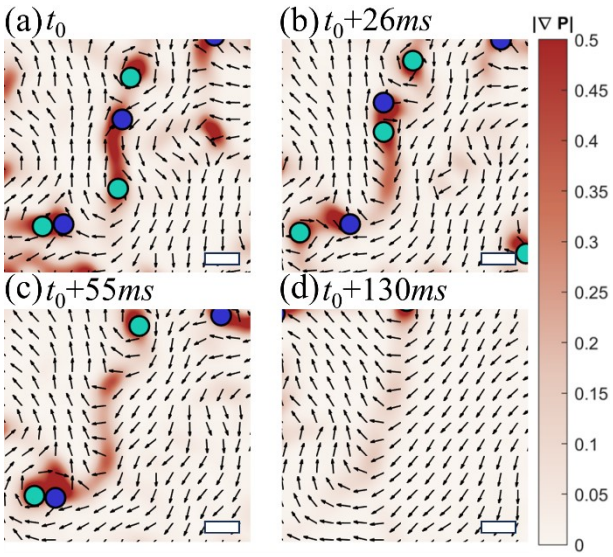


Fig.4 Annihilation of ±1 topological defects on domain walls and reconfiguration of flow fields. (a) Multiple pairs of defects are anchored on the distorted domain wall network. (b–c) Oppositely charged defects approach each other along the domain wall trajectories and annihilate. (d) After the defect pair annihilation, the originally disordered black arrows become aligned, and the corresponding domain walls significantly weaken and eventually vanish. The scale bars in (a-d) are 50 μm.